ACADEMIC PRESS

Journal of Solid State Chemistry 169 (2002) 24–34

JOURNAL OF SOLID STATE CHEMISTRY

www.academicpress.com

Static disorder from lone-pair electrons in $Bi_{2-x}M_xRu_2O_{7-y}$ ($M = Cu, Co$; $x = 0, 0.4$) pyrochlores

M. Avdeev,[a,*] M.K. Haas,[b] J.D. Jorgensen,[a] and R.J. Cava[b]

[a] *Argonne National Laboratory, Materials Science Division, Building 223, D-217 9700 S. Cass Ave. Argonne, IL 60439, USA*
[b] *Department of Chemistry and Princeton Materials Institute, Princeton University, Princeton, NJ 08540, USA*

Received 4 June 2002; received in revised form 16 July 2002; accepted 5 August 2002

Abstract

The crystal structures of $Bi_2Ru_2O_7$ and $Bi_{1.6}M_{0.4}Ru_2O_7$ ($M = Cu, Co$) pyrochlores are determined by Rietveld refinement of neutron powder diffraction data collected between 300 and 12 K. An appreciable oxygen non-stoichiometry, with no vacancy ordering, is found only in undoped $Bi_2Ru_2O_7$. In all three compounds, static displacive disorder of both the Bi and O′ sites is observed. This type of disorder has not been reported previously for $Bi_2Ru_2O_7$, and is proposed to be a common feature of $A_2B_2O_7$ pyrochlores having a lone electronic pair on the A-site cation. The electronic properties of $Bi_2Ru_2O_7$ are discussed in terms of calculated electronic band structure, local ruthenium coordination, and the static bismuth displacement.

Keywords: Pyrochlores; Neutron powder diffraction; Crystal structure; Band structure

1. Introduction

The pyrochlore ruthenates are widely studied because of their interesting electronic properties and technological importance as materials for thick-film resistors [1], catalysts [2], electrode materials [3], etc. The pyrochlore oxide $Bi_2Ru_2O_7$ exhibits temperature-independent Pauli paramagnetism and is weakly metallic [4]. In recent work [5], we have explored the effects on the magnetic properties of metal (Mn, Fe, Co, Ni, and Cu) doping on the Bi site in this compound. In this paper, we report the structural properties of the parent compound, $Bi_2Ru_2O_{7-y}$, and two of the doped compounds, $Bi_{2-x}M_xRu_2O_{7-y}$ ($M = Cu, Co; x = 0, 0.4$).

Compounds with the pyrochlore structure can be represented by the general formula $[A_2O'][B_2O_6]$ emphasizing that the structure consists of a rigid three-dimensional network of corner sharing BO_6 octahedra, with A and O′ atoms occupying interstitial sites, with O and O′ in the non-equivalent crystallographic sites 48f and 8b, respectively. Oxygen vacancy formation, if it occurs, prefers the interstitial O′ site rather than the O site. In the ideal structure, described by the $Fd3m$ (No. 227) cubic space group, the atoms are located mostly in special positions with fixed (x, y, z); the only positional variable is x(O). The chemical variables commonly used to modify the physical properties of these compounds are oxygen vacancy content and metal-site substitution [6–8].

Bismuth ruthenate $Bi_2Ru_2O_7$ was first prepared and electrically characterized by Bouchard et al. [4]. A cubic pyrochlore structure with $a = 10.2993(6)$ Å was reported, but no other structural information was given. Later, Horowitz et al. reported data for the "$Bi_2(Ru_{2-x}Bi_x)O_{7-y}$" solid solution [9]. A very similar cubic cell parameter ($a \sim 10.30$ Å) was found for the composition with $x = 0$. However, neither the details of the mechanism of the compensation of charge imbalance due to Bi/Ru substitution nor the amount of oxygen vacancies, y, were presented. In order to find the coordinates and occupancy of oxygen atom positions more precisely than those obtained by X-ray diffraction [10], Facer et al. studied $Bi_2Ru_2O_{7-y}$ using neutron powder diffraction [11]. The occupancy of the O′ site was found to be ~ 0.92, defining the composition as $Bi_2Ru_2O_{6.92}$. Additionally, the thermal parameter of the heavy bismuth cations was found to be abnormally high ($B_{eq}(Bi) \approx 1.5$ Å^2), which is more than five times higher than that of Ru. Static disorder of the Bi and an

*Corresponding author. Fax: +1-630-252-7777.
E-mail address: avdeev@anl.gov (M. Avdeev).

0022-4596/02/$ - see front matter
PII: S0022-4596(02)00007-5

underoccupied O′ site were suggested as a possible explanation for this, but no results for a disordered structural model were reported. A similar anomaly of the thermal parameter of the Bi atoms was found for $Bi_2Ru_2O_7$ in the course of studies of the $Bi_{2-x}M_xRu_2O_7$ (M = Y, Pr–Lu) system ($B_{eq}(Bi) = 0.9$ vs $B_{eq}(Ru) = 0.1$) [7,12] and for the analogous Ca-doped ruthenate ($B_{eq}(Bi/Ca) = 1.1$ Å^2 vs $B_{eq}(Ru) = 0.21$ Å^2) [13].

The 6*s* lone pair electrons of the Bi^{3+} cation, and the resulting effects on bonding to near-neighbor oxygen atoms, can explain subtle structural differences between $Bi_2Ru_2O_7$ and most other pyrochlore oxide compounds, such as those based on rare-earth elements [13]. In particular, the lone-pair bonding can explain the *A*-site disorder. This hypothesis is supported by the results of an X-ray single-crystal diffraction study of the pyrochlore-type tantalate with Tl^+, which is isoelectronic to Bi^{3+}, on the *A* site, $Tl_2Ta_2O_6$ [14]. For the ideal pyrochlore model with Tl^+ placed in the special position 16*d* (1/2,1/2,1/2), $B_{eq}(Tl^+)$ was found to be 7.02 Å^2 vs $B(Ta) = 0.26$ Å^2, and a Fourier difference map showed extra off-center electronic density. After displacing Tl^+ to a disordered (x, x, x) position ($x \sim 0.526$), the thermal parameter of Tl^+ dropped to more reasonable values 2–3 Å^2 vs $B_{eq}(Ta) = 0.70$ Å^2. Another evidence of the significant role of the 6*s* lone pair in the crystal chemistry of pyrochlores can be found by comparing the structural and bonding trends in a wide range of ruthenates [15] where, for Pb^{2+} and Bi^{3+}-based compounds, a pronounced deviation of the structural characteristics such as lattice parameter, oxygen positional parameter, and Ru–O–Ru angle from the correlations established for rare earth ruthenates was found. These observations guided the present study of the crystal structures of $Bi_2B_2O_7$ pyrochlores, with special attention to the positional and thermal parameters of the Bi and O′ sites.

We report here the results of a neutron powder diffraction study of bismuth ruthenate and the doped compounds $Bi_{2-x}M_xRu_2O_7$ (M = Cu, Co), whose properties are reported elsewhere [5]. Previous work on the electrical properties of the Cu- and Co-doped bismuth ruthenate gave only limited structural information [16]. In order to separate dynamic and static disorder, if any, data were collected at both room and low temperature. Time-of-flight diffraction data are especially suitable for such studies because of the availability of high Q data, which reduces the correlation between thermal and static displacement in structure refinement.

2. Synthesis, diffraction, and band structure calculations

Samples of the undoped bismuth ruthenate and $Bi_{2-x}M_xRu_2O_7$ (M = Cu, Co; $x = 0.4$) were prepared by conventional solid-state reaction of the oxides. Stoichiometric amounts of RuO_2, Co_3O_4, CuO, and Bi_2O_3 were thoroughly mixed and pressed into pellets. The samples were successively heated in air at 750°C for 1 day, 900°C for 1 day, 950°C for 3 days, and 975°C for 1 day, with intermediate grindings.

For the three samples, neutron powder diffraction data were collected at room temperature and 12 K on the Special Environment Powder Diffractometer [17] at the Intense Pulsed Neutron Source, Argonne National Laboratory. For the Co-doped ruthenate data were collected at two intermediate temperatures, 100 and 200 K, as well. The samples were contained in sealed thin-wall vanadium cans along with helium exchange gas except for room-temperature data collection from the Cu-doped sample which was suspended in the beam on a boron fiber to minimize background. Rietveld refinement was performed using the GSAS suite [18]. During the refinement of the structure of the doped $Bi_{2-x}M_xRu_2O_{7-y}$ compounds, the total occupancy of the *B* site was constrained to be 1, and the content of *M* was constrained to the nominal one (n(M@Bi) + n(M@Ru) = x, where n is the product of normalized site multiplicity and occupancy) since no evidence of M(2+) oxide segregation was observed.

Electronic band structure calculations utilized the LMTO-ASA codes of Anderson and coworkers [19], employing the local density approximation and the tetrahedral method of reciprocal space integration [20]. All relativistic effects, with the exception of spin–orbital coupling, are included in the method. The Ru 4*f*; Bi 6*d*, 5*f*; and O 2*s*, 3*p* orbitals were treated by a special downfolding procedure [21]. The number of k-points was incrementally increased until there was no change in the total energy, with a final total of 72 irreducible points from a grid of $12 \times 12 \times 12$ reducible points in each direction of the Brillouin zone.

3. Results and discussion

3.1. $Bi_2Ru_2O_7$

Structure refinement using the neutron powder diffraction data collected at room temperature was started with the ideal pyrochlore model (sp. gr. *Fd*3*m*) with x(O) being the only positional variable. Immediately, both bismuth and oxygen non-stoichiometry was seen. However, no evidence of oxygen vacancy ordering similar to that reported for a number of Pb^{2+}-based compounds [22–25] was observed. This is not surprising because, as was discussed recently by Ismunandar et al. [25], vacancy ordering typically occurs in $A_2B_2O_{7-y}$ pyrochlores for larger vacancy concentrations on the order of $y \approx 0.5$. In the present case, the vacancy concentration is much smaller. The thermal parameters

Table 1
Refined structural parameters for $Bi_{2-y}Ru_2O_{7-z}$ at room temperature, cubic space group *Fd*3*m* (No. 227), with Bi at 16*d* (1/2,1/2,1/2) (model 1) or 96*h* $(0, y, -y)$ (models 2 and 3) site, Ru at 16*c* (0,0,0) site, O at 48*f* $(x, 1/8, 1/8)$ site, O′ at 8*b* (3/8,3/8,3/8) (models 1 and 2) or 32*e* (x, x, x) (model 3) site. Numbers in parentheses are standard deviations of the last significant digit. Values with no standard deviations shown were not refined

	Model 1	Model 2	Model 3
a(Å)	10.28974(8)	10.28976(7)	10.28976(7)
x(Bi)	1/2	0	0
y(Bi)	1/2	0.23872(18)	0.23872(18)
z(Bi)	1/2	0.76128(18)	0.76128(18)
n(Bi@Bi)	1.90(1)	1.90(1)	1.90(1)
U_{iso}(Bi)(Å^2)	0.0186(3)	0.0077(8)	0.0078(8)
n(Ru@Ru)	2	2	2
U_{iso}(Ru)(Å^2)	0.0035(1)	0.0034(1)	0.0033(1)
x(O)	0.32652(6)	0.32649(6)	0.32649(6)
U_{iso}(O)(Å^2)	0.0081(1)	0.0080(1)	0.0080(1)
x(O′)	3/8	3/8	0.3820(15)
y(O′)	3/8	3/8	0.3820(15)
z(O′)	3/8	3/8	0.3820(15)
n(O′)	0.922(9)	0.931(9)	0.928(8)
U_{iso}(O′)(Å^2)	0.0183(6)	0.0189(6)	0.0135(25)
R_p(%)[a]	4.61	4.13	4.13
R_{wp}(%)[a]	8.23	7.79	7.79
χ^2	2.26	2.02	2.02

[a] Background subtracted.

Table 2
Refined structural parameters for $Bi_{2-y}Ru_2O_{7-z}$ at 12 K, cubic space group *Fd*3*m* (No. 227), with Bi at 16*d* (1/2,1/2,1/2) (model 1) or 96*h* $(0, y, -y)$ (models 2 and 3) site, Ru at 16*c* (0,0,0) site, O at 48*f* $(x, 1/8, 1/8)$ site, O′ at 8*b* (3/8,3/8,3/8) (models 1 and 2) or 32*e* (x, x, x) (model 3) site. Numbers in parentheses are standard deviations of the last significant digit. Values with no standard deviations shown were not refined

	Model 1	Model 2	Model 3
a(Å)	10.26994(7)	10.26995(7)	10.26995(7)
x(Bi)	1/2	0	0
y(Bi)	1/2	0.24008(17)	0.24008(17)
z(Bi)	1/2	0.75992(17)	0.75992(17)
n(Bi@Bi)	1.87(1)	1.88(1)	1.88(1)
U_{iso}(Bi)(Å^2)	0.0127(2)	0.0047(6)	0.0048(6)
n(Ru@Ru)	2	2	2
U_{iso}(Ru)(Å^2)	0.0023(1)	0.0021(1)	0.0021(1)
x(O)	0.32707(5)	0.32705(5)	0.32705(5)
U_{iso}(O)(Å^2)	0.0053(1)	0.0053(1)	0.0053(1)
x(O′)	3/8	3/8	0.3816(11)
y(O′)	3/8	3/8	0.3816(11)
z(O′)	3/8	3/8	0.3816(11)
n(O′)	0.903(8)	0.906(8)	0.904(8)
U_{iso}(O′)(Å^2)	0.0133(5)	0.0134(4)	0.0087(18)
R_p(%)[a]	6.86	6.46	6.46
R_{wp}(%)[a]	4.59	4.23	4.22
χ^2	3.10	2.81	2.80

[a] Background subtracted.

of Bi and O′ were found to be several times higher than those of Ru and O (Table 1, Model 1) as was previously reported for bismuth ruthenate [7,11,12] and other Bi^{3+}-based pyrochlores such as $Bi_2Ir_2O_{7-y}$ [24], $Bi_2Sn_2O_7$ [26], $Bi_2Rh_2O_{7-y}$ [27] when the structure was described with Bi atoms in the 16-fold (1/2,1/2,1/2) site.

Data collected at low temperature were compared with the room-temperature data in order to discriminate between dynamic and static disorder. As can be seen in Table 2 (Model 1), refinement using the low-temperature data with the ideal pyrochlore model resulted in values of thermal parameters of Bi and O′ much larger than those can be attributed to thermal vibrations at 12 K. Additionally, a Fourier difference map clearly showed extra off-center distorted donut-shaped scattering density around the Bi site indicating static displacive disorder. The same feature was observed in $Sn_{2-x}(Ta, Sn)_2O_{7-y}$ [28] and $Bi_{2-x}Ti_2O_{7-y}$ [29]. It was found in both of those cases that such a shape could not be described adequately by an anisotropic thermal parameter. Our attempt to model the observed scattering density with an anisotropic thermal parameter failed as well. Thus, a disordered model with displaced sites was used. There are two inequivalent sites that can be used to model the atomic displacements observed, i.e., 96*g*(x, x, z) and 96*h*$(0, y, -y)$. In the case of $Sn_{2-x}(Ta, Sn)_2O_{7-y}$, the former model was found to give slightly better refinement quality [28], while for $Bi_{2x}Ti_2O_{7-y}$ the latter model was reported as a better

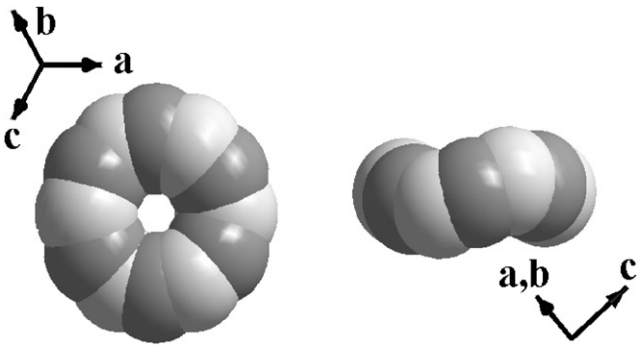

Fig. 1. Overlapping of the refined Bi atom positions for models in which Bi is displaced into disordered 96*g* (dark gray) or 96*h* (light gray) site.

choice [29]. We tested both models and found no statistically significant difference in agreement factors. Examination of the arrangement of the 96*g* and 96*h* sites in real space revealed that in fact they overlap, supplementing each other in order to simulate a continuous distribution of scattering density around the ideal position (1/2,1/2,1/2) as shown in Fig. 1. However, the essential features of the disorder are adequately represented by either model. We describe the structure with the 96*h*$(0, y, -y)$ disordered site model which has one variable less. As can be seen in Table 2 (Model 2), the refinement using the model with disordered Bi sites resulted in both more reasonable thermal parameters and better refinement quality.

However, the thermal parameter of O′ was still too high for such a low temperature and the Fourier difference map indicated extra scattering density along the (111) direction toward the nearest-neighbor disordered Bi position. Use of an anisotropic thermal parameter cannot provide an acceptable fit because the thermal parameter is isotropic by symmetry for this site. Thus, the ideal 8*b* (3/8,3/8,3/8) site was split to a disordered 32*e* (x, x, x) site. The results of the refinement using this model are summarized in Table 2 (Model 3). The additional improvement in the quality of the refinement is just above the formal limit of statistical significance and the decrease of the thermal parameter of O′ to a physically sensible value supports the correctness of this model. The high standard deviation of the thermal parameter is caused by correlation with the positional parameter and the occupancy as is common in such refinement models for non-stoichiometric disordered materials. The character of the O′ site splitting looks physically reasonable considering what one would expect for the Cu_2O-like Bi_2O' network. The disorder of Bi atoms in the direction perpendicular to Bi–O′ bonds induces disorder in the oxygen site as shown in Fig. 2. The final Rietveld refinement plot is presented in Fig. 3. It should be noted that we have also tested the model with coexisting ideal 16*d* (1/2,1/2,1/2) and disordered 96*g* (x, x, z) and/or 96*h* $(0, y, -y)$ positions for Bi similar to that reported for $Tl_2Ta_2O_6$ [14]. However, the refinement process was unstable and gave a negative occupancy for the 16*d* site.

The same two models, i.e., model 2 with only the Bi site disordered and model 3 with both Bi and O′ sites disordered, were applied to refinements using the room-temperature diffraction data for bismuth ruthenate. The results are summarized in Table 1 (Models 2 and 3, respectively). Again, splitting of both the Bi and O′ sites resulted in substantial decreases of their thermal parameters, yielding values more comparable to those for Ru and O. The small difference in the refined values for the O′ site occupancy obtained from low- and room-temperature data cannot be real and, thus, reflects the real error of the structural refinement. The refinements give an average composition of $Bi_{1.89(1)}Ru_2O_{6.92(1)}$. The bismuth and oxygen non-stoichiometry is very close to that reported for $Bi_{1.95}Rh_2O_{6.83}$ [28] and $Bi_{1.89}(GaSb)O_{6.84}$ [25]. The final Rietveld plot is presented in Fig. 4.

3.2. $Bi_{2-x}M_xRu_2O_7$ $(M = Co, Cu)$

For the ruthenate with nominal composition $Bi_{1.6}Co_{0.4}Ru_2O_7$, a refinement using the model with Bi in 96*h* and O′ in 32*e* sites converged smoothly to the results presented in Table 3. A second phase of ruthenium dioxide [30] was found in a trace amount with a concentration averaged over the four runs at different temperatures of 0.46(4) wt%. This confirms the expected doping into the *A* site because the case of Co substitution only for Ru would give about 8 wt% of RuO_2 impurity. Also, during the refinement, Co was allowed to substitute at both the Bi and Ru sites. The substitution of Co for Ru refined to be about 3(1)% which is comparable to the amount of Ru segregated into the RuO_2 impurity phase. The total composition

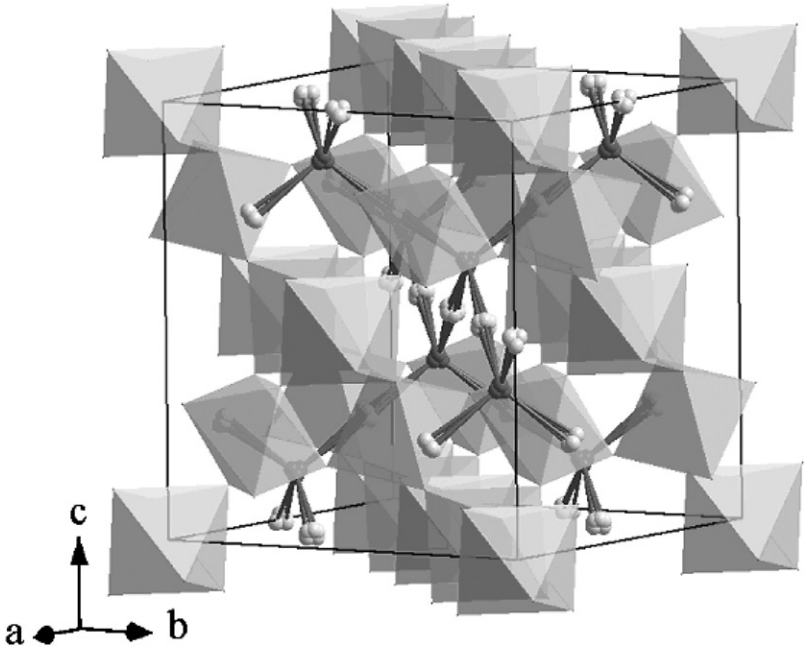

Fig. 2. View of the $Bi_{2-x}Ru_2O_{7-y}$ crystal structure as a network of the corner-sharing RuO_6 octahedra penetrated by disordered Bi_2O' Cu_2O-like network. The dark spheres are O′ atoms and light spheres are Bi atoms.

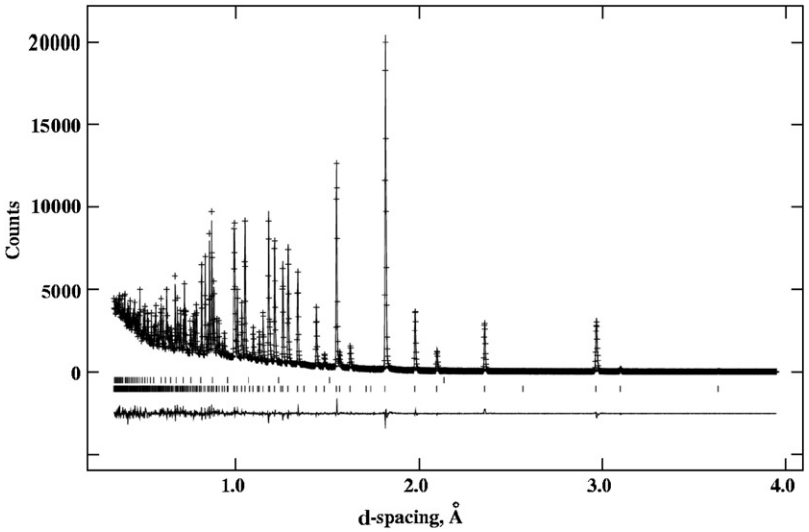

Fig. 3. Rietveld refinement plot showing the observed (+) and calculated (solid line) diffraction data and their difference for $Bi_{1.89}Ru_2O_{6.92}$ at 12 K. Upper ticks mark very weak reflections of the vanadium can; lower ticks mark the $Bi_{1.89}Ru_2O_{6.92}$ reflections.

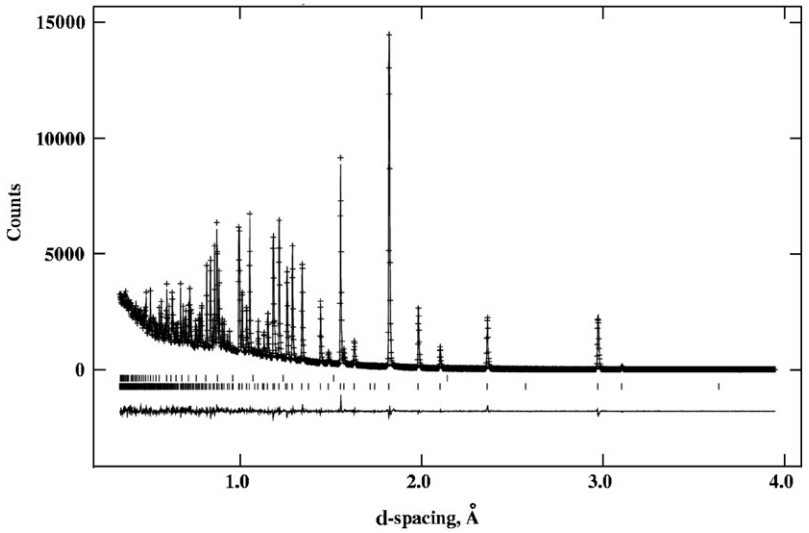

Fig. 4. Rietveld refinement plot showing the observed (+) and calculated (solid line) diffraction data and their difference for $Bi_{1.89}Ru_2O_{6.92}$ at room temperature. Upper ticks mark very weak reflections of the vanadium can; lower ticks mark the $Bi_{1.89}Ru_2O_{6.92}$ reflections.

using the occupancies averaged over the runs at four different temperatures is $(Bi_{1.58(2)}Co_{0.35(7)})$ $(Ru_{1.95(1)}Co_{0.05(1)})O_6O'_{0.98(1)}$. The agreement between observed and calculated diffraction patterns is shown by the Rietveld plot for the room temperature data, Fig. 5. The refinement results are summarized in Table 3.

The refined cell parameter at room temperature is in good agreement with that previously reported for $Ru_{1.6}Co_{0.4}Ru_2O_{7-y}$ [16]. The thermal expansion (see Fig. 6) decreases slightly at low temperature, similar to that reported for $Cd_2Ru_2O_7$ [31] and $Bi_{0.5}Nd_{1.5}Ru_2O_7$ [32]. The behaviors of other structural parameters versus temperature, including those that define the pattern of static disorder, are shown in Figs. 7 and 8.

For the Cu-doped ruthenate, no RuO_2 impurity peaks were visible in the data. For both room and low temperature, the O′ 32*e* (x, x, x) site was found to be fully occupied; therefore, the occupancy was fixed to 0.25 for the final refinements. No detectable substitution of Cu for Ru was observed and the refined chemical composition was found to be $Bi_{1.60(5)}Cu_{0.40(4)}Ru_2O_7$ which agrees with the nominal composition.

The agreement between observed and calculated diffraction patterns is illustrated by the Rietveld plot

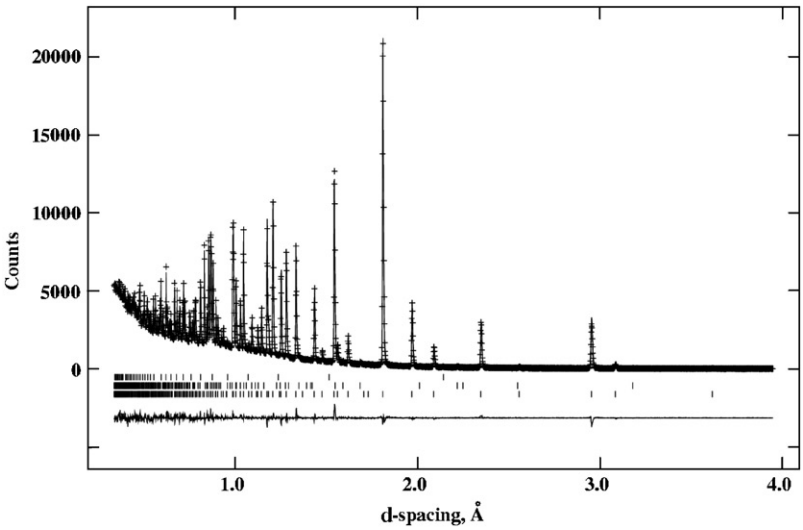

Fig. 5. Rietveld refinement plot showing the observed (+) and calculated (solid line) diffraction data and their difference for $Bi_{1.58}Co_{0.40}Ru_{1.95}O_{6.98}$ at room temperature. Upper ticks mark very weak reflections of the vanadium can; middle ticks mark RuO_2; lower ticks mark the $Bi_{1.58}Co_{0.40}Ru_{1.95}O_{6.98}$ reflections.

Table 3
Refined structural parameters for $Bi_{1.6}Co_{0.4}Ru_2O_7$, cubic space group *Fd*3*m* (No. 227), with Bi (or Co) disordered at 96*h* $(0, y, -y)$ site, Ru (or Co) at 16*c* (0,0,0), O at 48*f* $(x, 1/8, 1/8)$, and O′ disordered at a 32*e* (x, x, x) site. Constraints used for the refinement were $n(\text{Ru@Ru}) + n(\text{Cu@Ru}) = 2$ and $n(\text{Co@Bi}) + n(\text{Co@Ru}) = 0.4$. Numbers in parentheses are standard deviations of the last significant digit. Values with no standard deviations shown were not refined

	295 K	200 K	100 K	12 K
a(Å)	10.22755(3)	10.21980(3)	10.21380(3)	10.21108(3)
y(Bi)	0.23754(15)	0.23797(15)	0.23833(15)	0.23862(14)
n(Bi@Bi)	1.60(2)	1.56(2)	1.58(2)	1.57(2)
n(Co@Bi)	0.36(6)	0.30(7)	0.36(7)	0.37(7)
U_{iso}(Bi)(Å^2)	0.0077(5)	0.0064(4)	0.0052(4)	0.0041(4)
n(Ru@Ru)	1.96(1)	1.91(1)	1.95(1)	1.97(1)
n(Co@Ru)	0.04(1)	0.09(1)	0.05(1)	0.03(1)
U_{iso}(Ru)(Å^2)	0.00307(11)	0.00273(11)	0.00207(10)	0.00188(10)
x(O)	0.32631(5)	0.32646(5)	0.32665(5)	0.32678(5)
U_{iso}(O)(Å^2)	0.00744(9)	0.00631(8)	0.00542(7)	0.00505(7)
x(O′)	0.38787(14)	0.38800(14)	0.38813(13)	0.38824(13)
n(O′)	1.00(1)	0.96(1)	0.98(1)	0.98(1)
U_{iso}(O′)(Å^2)	0.015(1)	0.013(1)	0.011(1)	0.0092(9)
R_p(%)[a]	3.81	3.92	3.95	4.08
R_{wp}(%)[a]	5.62	5.83	5.81	5.85
χ^2	2.49	2.63	2.76	2.91

[a] Back subtracted.

for the room temperature data in Fig. 9. The refinement results are summarized in Table 4.

4. Electronic structure

The electronic properties of the ruthenate pyrochlores are not comprehensively understood [33]. $Bi_2Ru_2O_7$ and $Pb_2Ru_2O_{6.5}$ are weakly metallic, displaying temperature-independent resistivities over a broad temperature range. Conversely, $Y_2Ru_2O_7$ and the $Ln_2Ru_2O_7$ series are insulators, although isostructural and isoelectronic to their metallic counterparts. Previous publications consider the small Ru–O–Ru bond angle for lanthanide and yttrium pyrochlores as a possible explanation for their decreased conduction [34,35]. As bond angle decreases, orbital overlap will also decrease, resulting in a narrowed band and decreased mobility. However, the difference in Ru–O–Ru bond angle between metallic $Bi_2Ru_2O_7$ and non-metallic $Pr_2Ru_2O_7$ is less than 2°, making it unlikely that this is the sole reason for the difference in properties. It has also been proposed that

hybridization of Bi and Ru states present at the Fermi energy in $Bi_2Ru_2O_7$ leads to a wider conduction band relative to pyrochlores with lanthanide *A*-site elements [36]. Thus, previous electronic structure calculations investigated the potential influence of *A*-site (Bi, Y, Tl) cation hybridization in ruthenium pyrochlores [37].

Our neutron refinement study of $Bi_2Ru_2O_7$ provides new insight into the detailed crystal structure, and allows us to examine an additional origin for the differences in electronic behavior. We examine in detail the local coordination environment of ruthenium and present the results of electronic band structure calculations. Additionally, trigonal symmetry in the general pyrochlore structure is expected to have an effect on electronic structure [38]. We apply this postulate to $Bi_2Ru_2O_7$ specifically.

The RuO_6 coordination polyhedron in $Bi_2Ru_2O_7$ has been described as a regular octahedron. More precisely, however, the symmetry is trigonal antiprismatic, resulting from trigonal compression along a three-fold axis (Fig. 10a). The degree of compression can be measured by the angle (α) between the three-fold symmetry axis and the Ru–O bond. The value α in the pyrochlore structure also determines the Ru–O–Ru bond angle. In an ideal octahedron, $\alpha = 54.7^\circ$, while in $Bi_2Ru_2O_7$, $\alpha \sim 58.5^\circ$. In addition, ruthenium in $Bi_2Ru_2O_7$ has six bismuth nearest neighbors equidistant at ~ 3.6 Å, arranged in a planar hexagon perpendicular to the RuO_6 three-fold axis (Fig. 10b), as well as six trigonally symmetric Ru nearest neighbors equidistant at ~ 3.6 Å (three above the bismuth plane, three below

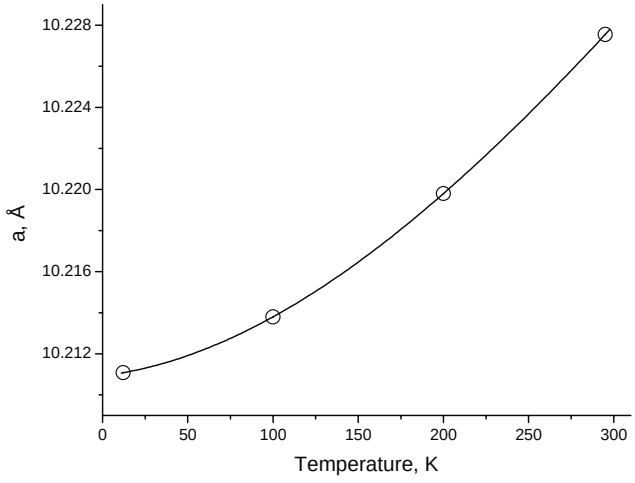

Fig. 6. Cubic cell parameter of $Bi_{1.58}Co_{0.40}Ru_{1.95}O_{6.9}$ versus temperature. Error bars are smaller than the symbols. The curve is a guide to the eye.

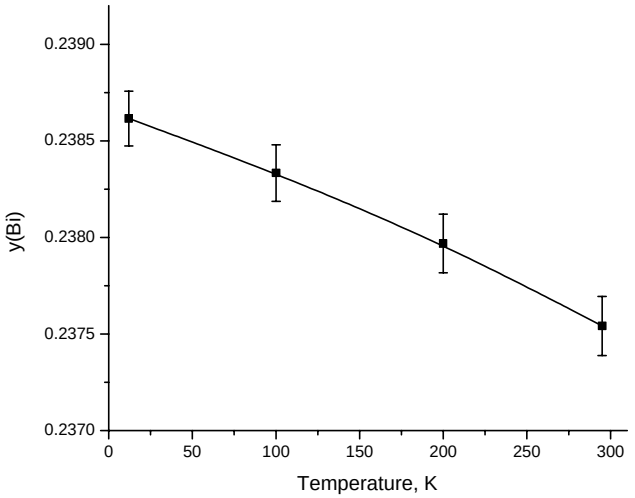

Fig. 8. *Y* Coordinate for the Bi $96h$ $(0, y, -y)$ site in $Bi_{1.58}Co_{0.40}Ru_{1.95}O_{6.98}$ versus temperature. Curve is a guide for the eye.

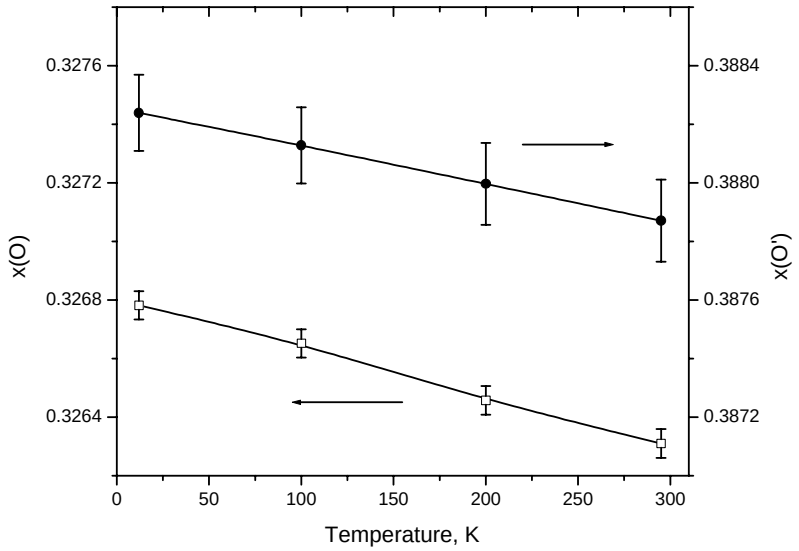

Fig. 7. *x* Coordinates for the O $48f$ $(x, 1/8, 1/8)$ and O′ $32e$ (x, x, x) sites in $Bi_{1.58}Co_{0.40}Ru_{1.95}O_{6.98}$ versus temperature. Curves are guide for the eye.

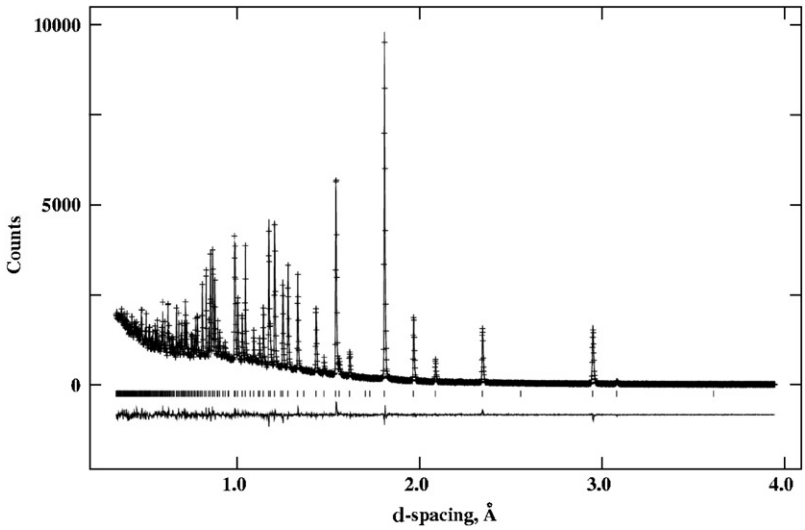

Fig. 9. Rietveld refinement plot showing the observed (+) and calculated (solid line) diffraction data and their difference for $Bi_{1.60}Cu_{0.40}Ru_2O_7$ at room temperature. Ticks mark the $Bi_{1.60}Cu_{0.40}Ru_2O_7$ reflections.

Table 4
Refined structural parameters for $Bi_{1.6}Cu_{0.4}Ru_2O_7$, cubic space group *Fd3m* (No. 227), with Bi (or Cu) disordered at 96*h* $(0, y, -y)$ site, Ru (or Cu) at 16*c* (0,0,0), O at 48*f* $(x, 1/8, 1/8)$, and O′ disordered at a 32*e* (x, x, x) site. Constraints used for the refinement were $n(\text{Ru@Ru}) + n(\text{Cu@Ru}) = 2$ and $n(\text{Cu@Bi}) + n(\text{Cu@Ru}) = 0.4$. Numbers in parentheses are standard deviations of the last significant digit. Values with no standard deviations shown were not refined

	295 K	12 K
a(Å)	10.21463(8)	10.20054(9)
y(Bi)	0.23727(18)	0.23853(21)
n(Bi@Bi)	1.62(1)	1.57(1)
n(Cu@Bi)	0.40(5)	0.40(5)
U_{iso}(Bi)(Å^2)	0.0094(6)	0.0036(7)
n(Ru@Ru)	2	2
n(Cu@Ru)	0	0
U_{iso}(Ru)(Å^2)	0.0035(1)	0.0021(2)
x(O)	0.32584(6)	0.32630(7)
U_{iso}(O)(Å^2)	0.0080(1)	0.0050(1)
x(O′)	0.3897(4)	0.3901(4)
n(O′)	1	1
U_{iso}(O′)(Å^2)	0.0226(19)	0.0144(17)
R_p(%)[a]	4.01	3.42
R_{wp}(%)[a]	8.07	4.97
χ^2	1.56	1.80

[a] Background subtracted.

the bismuth plane). Thus, the overall coordination around ruthenium in the pyrochlore is trigonal, and a great deal more anisotropic than the *A*-site coordination around the *B*-metal in the perovskite structure. The resulting local point symmetry of the ruthenium coordination is lowered from O_h, which is present in perovskite-based structures, to D_{3d}. Fig. 10c illustrates that for Ru^{4+}, this distortion can cause what would be a partially filled band (O_h) to split into a completely filled band and an empty band (D_{3d}) [38,39].

Electronic band structure calculations were performed for $Bi_2Ru_2O_7$ in space group *Fd3m*. The positions of Ru and O were taken from Table 1. The static displacements of Bi and O′, however, were not included in the calculation: instead, the two atoms were placed in positions 16*d* and 8*b*, respectively. The resulting electronic density of states (DOS) as a function of energy is presented in Fig. 11. The ruthenium t_{2g} states are split in good agreement with that expected of D_{3d} symmetry. Thus, the assignment of "octahedral" symmetry for ruthenium in the pyrochlore structure is not a suitable description. The Fermi energy (E_F) lies at the top of a filled band (e'_g) of four electrons per ruthenium, while directly above E_F an empty band (a_{1g}) is comprised of two electrons per ruthenium. Therefore, the density of states at the Fermi energy is lowered almost to zero, and the pyrochlore can be classified as a semi-metal. In fact, the band splitting remains pronounced even when a theoretical model is used for $Bi_2Ru_2O_7$, in which the RuO_6 octahedra are perfect; with $\alpha = 54.7^\circ$ and O(1) in position 0.3125, 1/8, 1/8. The persistence of the splitting reflects the significant influence of the local bismuth and ruthenium nearest neighbor coordination on the ruthenium crystal field, and that t_{2g} band splitting is inherent to the pyrochlore framework.

The results presented in Fig. 11 are in good general agreement with those reported by Ishii and Oguchi [37]. However, the oxygen positional parameter they employ for $Bi_2Ru_2O_7$ was obtained by powder X-ray diffraction refinement, and is significantly different from ours. The result includes an over-estimation of the calculated value of $N(E_F)$ in their calculation. Neutron diffraction more accurately detects the presence of oxygen; therefore the parameters employed in the present study are more accurate.

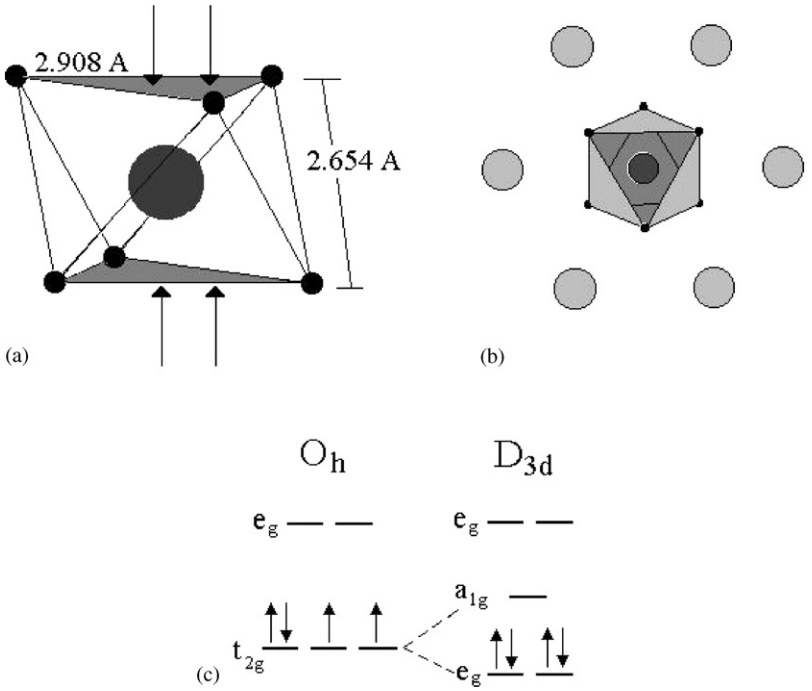

Fig. 10. (a) RuO_6 trigonal antiprism in $Bi_2Ru_2O_7$. (b) View down 3-fold symmetry axis of RuO_6 trigonal antiprism. Light gray spheres are Bi atoms in position 16*d*, in a plane perpendicular to the 3-fold axis. (c) Expected *d*-orbital splitting for Ru^{4+} in O_h and D_{3d} symmetry in $Bi_2Ru_2O_7$.

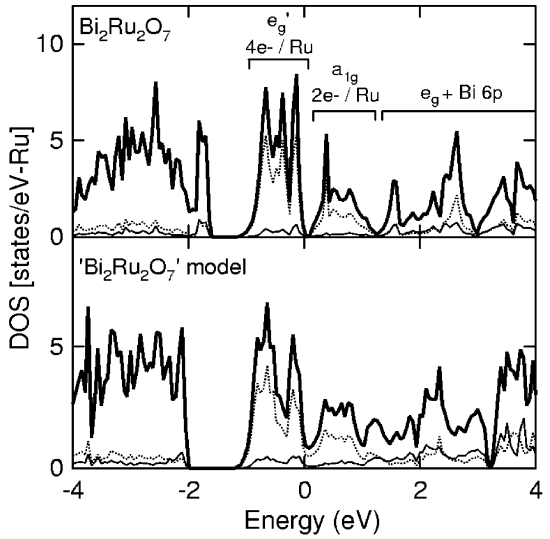

Fig. 11. Calculated density of states for $Bi_2Ru_2O_7$ (top panel), and for an undistorted model of $Bi_2Ru_2O_7$ (bottom panel) in which the octahedra are regular and Bi and O are in positions 1/2, 1/2, 1/2 and 0.3125, 1/8, 1/8, respectively. The Fermi energy is set to zero. Thick solid lines plot the total density of states, dotted lines plot the Ru partial density of states, and thin solid lines plot the *A*-cation partial density of states. Ru–O–Ru bond angles for the three structures are 133° and 141° (from top to bottom).

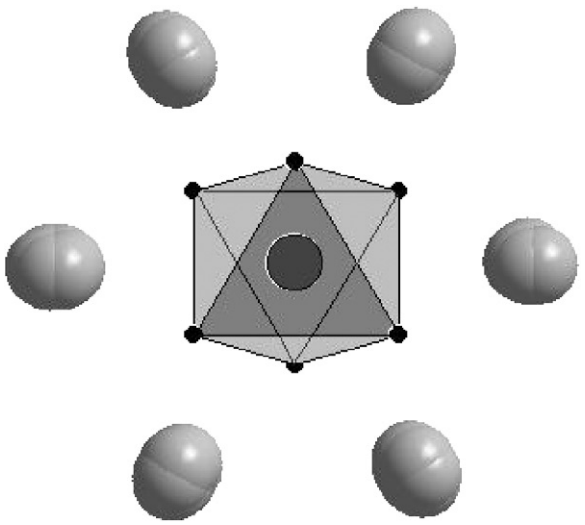

Fig. 12. View of RuO_6 trigonal antiprism down the 3-fold axis of symmetry. Light gray spheres are bismuth atoms displaced to position 96*g*.

It is also important to consider the effect of the bismuth static displacement observed in our structural study on the electronic properties of $Bi_2Ru_2O_7$. Computationally, we are unable to include partial occupancy, and therefore have not performed calculations with Bi in the displaced 96*g* or 96*h* sites. However, we qualitatively examine the effect of the observed Bi static displacement on electronic structure. Fig. 12 illustrates the ruthenium coordination with bismuth in crystallographic site 96*g*. Each ideal position (Fig. 10b) is split into six displaced sites, such that only one of the six sites can be occupied at a time. The average symmetry is unchanged by the displacement and the space group

relative to the ideal pyrochlore structure is equivalent. However, in a local picture, the D_{3d} symmetry at each individual ruthenium center is destroyed by the bismuth displacement. Thus, we expect the band splitting outlined in Fig. 10c to be less pronounced in disordered $Bi_2Ru_2O_7$, and the density of states at E_F to be higher than the calculation predicts. Indeed, an experimental value of $N(E_F)$ is reported as ~ 4 states/eV-Ru, and the compound is a poor metal [40]. Plausibly, the static displacement of Bi observed in $Bi_2Ru_2O_7$ is due to its lone-electronic pair. Therefore, we would expect other pyrochlores with *A*-site lone pairs, and thus *A*-site disorder, to have higher $N(E_F)$ values and higher conductivity than those without *A*-site lone pairs. The fact that $Y_2Ru_2O_7$ and $Ln_2Ru_2O_7$ are insulating while isoelectronic $Bi_2Ru_2O_7$ and $Pb_2Ru_2O_{6.5}$ are weakly metallic is in agreement with this hypothesis, though we do not propose that this is the only factor in that difference.

T_{2g} band splitting is intrinsic to the D_{3d} *B*-site symmetry in the pyrochlore structure. In $Bi_2Ru_2O_7$, with 4*d*-electrons per ruthenium, the splitting leads to a low value of $N(E_F)$ and semi-metallic character. Additionally, the Fermi level in $Bi_2Ru_2O_7$ lies in a sharp valley in the density of states, and subtle changes such as *A*-site disorder can have a dramatic effect on the electronic properties.

5. Conclusions

Our structural refinements for bismuth ruthenate and its Co- and Cu-doped derivatives revealed static displacement of both Bi and O′ atoms from the ideal pyrochlore positions into disordered sites. We conclude that this disorder is related to the stereochemical activity of the lone electronic pair of Bi^{3+}. Similar static disorder was found in other Bi^{3+}- [29,41], Tl^{+}- [14], and Sn^{2+}-based [28,42] pyrochlores. We believe that such disorder is likely to be present in most pyrochlore compounds in which the *A* site is occupied by a cation having an s^2 lone electron pair. If this hypothesis is correct, structural refinements for such compounds with an ideal pyrochlore model will show abnormally high thermal parameters at all temperatures for both the *A*-site cation and O′ oxygen anion. We note that off-center displacement of *A*-site cations can also occur when the *A* site is occupied by a small transition metal, because the *A*-site cavity is clearly too big for them to be placed in the ideal center position.

Additionally, electronic band structure calculations for $Bi_2Ru_2O_7$ were performed. We observe that D_{3d} ruthenium symmetry, as well as the disruption of the local symmetry by static *A*-site cation disorder, are additional factors in determining the electronic behavior of Ru^{4+} pyrochlores.

Acknowledgments

The work at Argonne National Laboratory was supported by the US Department of Energy, Division of Basic Energy Sciences, contract No. W-31-1009-ENG-38. The work at Princeton University was supported by National Science Foundation Grant DMR-9809483. The authors thank Donald McClure and Andrew Bocarsly for sharing their insights into crystal field theory, and Simine Short for assistance during SEPD measurement.

References

[1] P.F. Garcia, A. Ferreti, A. Suna, J. Appl. Phys. 53 (1982) 5282.
[2] H.S. Horowitz, J.M. Longo, H.H. Horowitz, J. Electrochem. Soc. 130 (1983) 1851.
[3] T. Takeda, R. Kanno, Y. Kawamoto, Y. Takeda, O. Yamamoto, J. Electrochem. Soc. 147 (2000) 1730.
[4] R.J. Bouchard, J.L. Gillson, Mater. Res. Bull. 6 (1971) 669.
[5] M.K. Haas, R.J. Cava, M. Avdeev, J.D. Jorgensen, Phys. Rev. B, to appear.
[6] R.E. Carbonio, J.A. Alonso, J.L. Martinez, J. Phys.: Condens. Matter 11 (1999) 361.
[7] R. Kanno, Y. Takeda, T. Yamamoto, Y. Kawamoto, O. Yamamoto, J. Solid State Chem. 102 (1993) 106.
[8] H. Kobaysahi, R. Kanno, Y. Kawamoto, T. Kamiyama, F. Izumi, A.W. Sleight, J. Solid State Chem. 114 (1995) 15.
[9] H.S. Horowitz, J.M. Longo, J.T. Lewandowski, Mater. Res. Bull. 16 (1981) 489.
[10] F. Abraham, G. Nowogrocki, D. Thomas, C.R. Acad. Sci. Fr., Ser. C 279 (1975) 279.
[11] G.R. Facer, M.M. Elcombe, B.J. Kennedy, Aust. J. Chem. 46 (1993) 1897.
[12] T. Yamamoto, R. Kanno, Y. Takeda, O. Yamamoto, Y. Kawamoto, M. Takano, J. Solid State Chem. 109 (1994) 372.
[13] B.J. Kennedy, J. Solid State Chem. 119 (1995) 254.
[14] M. Ganne, M. Tournoux, Mater. Res. Bull. 10 (1975) 1313.
[15] B.J. Kennedy, T. Vogt, J. Solid State Chem. 126 (1996) 261.
[16] E. Beck, S. Kemmler-Sack, Mater. Res. Bull. 21 (1986) 307.
[17] J.D. Jorgensen, J. Faber Jr., J.M. Carpenter, R.K. Crawford, J.R. Haumann, R.L. Hitterman, R. Kleb, G.E. Ostrowski, F.J. Rotella, T.G. Worlton, J. Appl. Crystallogr. 22 (1989) 321.
[18] A.C. Larson, R.B. Von Dreele, Los Alamos National Laboratory Report, No. LAUR-86-748, 1987.
[19] O.K. Anderson, O. Jepsen, The Stuttgart TB-LMTO-ASA Program, version 47c, Phys. Rev. Lett. 53 (1984) 2571; O.K. Anderson, Z. Pawlowska, O. Jepsen, Phys. Rev. B 34 (1986) 5253.
[20] O. Jepsen, O.K. Anderson, Solid State Commun. 9 (1971) 1763; P. Blochl, O. Jepsen, O.K. Anderson, Phys. Rev. B 49 (1994) 16 223.
[21] W.R.L. Lambrecht, O.K. Anderson, Phys. Rev. B 29 (1984) 5965.
[22] R.A. Beyerlein, H.S. Horowitz, J.M. Longo, M.E. Leonowicz, J.D. Jorgensen, F.J. Rotella, J. Solid State Chem. 51 (1984) 253.
[23] J.A. Alonso, C. Cascales, I. Rasines, J. Pannetier, Acta Crystallogr. C 45 (1989) 3.
[24] B.J. Kennedy, J. Solid State Chem. 123 (1996) 14.
[25] Ismunandar, B.J. Kennedy, B.A. Hunter, Mater. Res. Bull. 34 (1999) 1263.
[26] Ismunandar, B.J. Kennedy, B.A. Hunter, T. Vogt, J. Solid State Chem. 131 (1997) 317.
[27] B.J. Kennedy, Mater. Res. Bull. 32 (1997) 479.

[28] T. Birchall, A.W. Sleight, J. Solid State Chem. 12 (1975) 118.
[29] I. Radosavljevic, J.S.O. Evans, A.W. Sleight, J. Solid State Chem. 136 (1998) 63.
[30] J. Haines, J.M. Leger, O. Schulte, S. Hull, Acta Crystallogr. B 53 (1997) 880.
[31] R. Wang, A.W. Sleight, Mater. Res. Bull. 33 (1998) 1005.
[32] M.D. Field, B.J. Kennedy, B.A. Hunter, T. Vogt, J. Solid State Chem. 144 (1999) 467.
[33] A.K. Cheetham, P. Day, Solid State Chemistry Techniques, Clarendon Press, Oxford, 1988.
[34] B.J. Kennedy, Physica B 241 (1998) 303.
[35] K.S. Lee, D.K. Seo, M.H. Whangbo, J. Solid State Chem. 131 (1977) 405.
[36] P.A. Cox, Transition Metal Oxides, Clarendon Press, Oxford, 1992, pp. 225–232.
[37] F. Ishii, T. Oguchi, J. Phys. Soc. Japan 69 (2000) 526.
[38] M.A. Subramanian, G. Aravamudan, G.V. Subba Rao, Prog. Solid State Chem. 15 (1983) 55.
[39] M. Gerloch, R.C. Slade, Ligand-Field Parameters, University Press, Cambridge, 1973, pp. 60–80.
[40] P.A. Cox, R.G. Egdell, J.B. Goodenough, A. Hamnett, C.C. Naish, J. Phys. C 16 (1983) 6221.
[41] R.H. Jones, K.S. Knight, J. Chem. Soc., Dalton Trans. 15 (1997) 2551.
[42] L.P. Cruz, J.M. Savariault, J. Rocha, Acta Crystallogr. C 57 (2001) 1001.